

# Solid-core photonic bandgap fibers for cladding-pumped Raman amplification

Benjamin Ward\*

Air Command and Staff College, Air University, 225 Chennault Circle, Maxwell Air Force Base, Alabama, 36112, USA

\*benjamin.ward.1@us.af.mil

**Abstract:** Cladding-pumped solid-core photonic bandgap Raman fiber amplifiers are analyzed theoretically as possible candidates for power scaling. An example fiber design with a mode field diameter of 46  $\mu\text{m}$  and a cladding diameter of 250  $\mu\text{m}$  is calculated to exhibit 0.12 dB/km of confinement loss at the first Stokes wavelength and  $>10$  dB/m at the second Stokes wavelength for a pump wavelength of 1.567  $\mu\text{m}$  while maintaining low loss and large mode area in realistic coiling configurations. A Raman amplifier based on this fiber with 85 kW of output power, 78% optical conversion efficiency, a maximum heat load of 130 W/m, and a length of 235 m is simulated.

©2011 Optical Society of America

**OCIS codes:** (140.3510) Lasers, fiber; (140.3550) Lasers, Raman; (290.5910) Scattering, stimulated Raman; (140.4480) Optical amplifiers; (060.2280) Fiber design and fabrication; (060.5295) Photonic crystal fibers.

---

## References and links

1. J. W. Dawson, M. J. Messerly, R. J. Beach, M. Y. Shverdin, E. A. Stappaerts, A. K. Sridharan, P. H. Pax, J. E. Heebner, C. W. Siders, and C. P. J. Barty, "Analysis of the scalability of diffraction-limited fiber lasers and amplifiers to high average power," *Opt. Express* **16**(17), 13240–13266 (2008), <http://www.opticsinfobase.org/oe/abstract.cfm?URI=oe-16-17-13240>.
2. J. S. Kim, C. Codemard, Y. Jeong, J. Nilsson, and J. K. Sahu, "High power continuous-wave Yb-doped fiber laser with true single-mode output using W-type structure," in *Conference on Lasers and Electro-Optics*, (Optical Society of America, 2006). <http://dx.doi.org/10.1109/CLEO.2006.4628264>.
3. L. Zenteno, J. Wang, D. Walton, B. Ruffin, M. Li, S. Gray, A. Crowley, and X. Chen, "Suppression of Raman gain in single-transverse-mode dual-hole-assisted fiber," *Opt. Express* **13**(22), 8921–8926 (2005), <http://www.opticsinfobase.org/oe/abstract.cfm?URI=OPEX-13-22-8921>.
4. S. Blin, L. Provino, N. Traynor, A. Mugnier, D. Pureur, and T. Chartier, "Design of all-solid photonic-bandgap fibers for Raman-free propagation," *Lasers and Electro-Optics 2009 and the European Quantum Electronics Conference. CLEO Europe - EQEC 2009. European Conference on*, pp.1, 14–19 June 2009.
5. A. Argyros, T. Birks, S. Leon-Saval, C. M. B. Cordeiro, and P. St J Russell, "Guidance properties of low-contrast photonic bandgap fibres," *Opt. Express* **13**(7), 2503–2511 (2005), <http://www.opticsinfobase.org/oe/abstract.cfm?URI=oe-13-7-2503>.
6. B. G. Ward, C. Robin, and M. Culpepper, "Photonic crystal fiber designs for power scaling of single-polarization amplifiers," *Proc. SPIE* **6453**, 645307, 645307-9 (2007), <http://dx.doi.org/10.1117/12.717326>.
7. T. Kokki, J. Koponen, M. Laurila, and C. Ye, "Fiber amplifier utilizing an Yb-doped large-mode-area fiber with confined doping and tailored refractive index profile," *Proc. SPIE* **7580**, 758016, 758016-9 (2010), <http://dx.doi.org/10.1117/12.842404>.
8. J. Ji, C. A. Codemard, M. Ibsen, J. K. Sahu, and J. Nilsson, "Analysis of the conversion to the first Stokes in cladding-pumped fiber Raman amplifiers," *IEEE J. Sel. Top. Quantum Electron.* **15**(1), 129–139 (2009), <http://dx.doi.org/10.1109/JSTQE.2008.2010229>.
9. J. E. Heebner, A. K. Sridharan, J. W. Dawson, M. J. Messerly, P. H. Pax, M. Y. Shverdin, R. J. Beach, and C. P. J. Barty, "High brightness, quantum-defect-limited conversion efficiency in cladding-pumped Raman fiber amplifiers and oscillators," *Opt. Express* **18**(14), 14705–14716 (2010), <http://www.opticsinfobase.org/oe/abstract.cfm?URI=oe-18-14-14705>.
10. J. Ji, C. A. Codemard, and J. Nilsson, "Analysis of spectral bendloss filtering in a cladding-pumped W-type fiber Raman amplifier," *J. Lightwave Technol.* **28**(15), 2179–2186 (2010), <http://dx.doi.org/10.1109/JLT.2010.2052786>.
11. N. Shibata, M. Horigudhi, and T. Eda, "Raman spectra of binary high-silica glasses and fibers containing GeO<sub>2</sub>, P<sub>2</sub>O<sub>5</sub> and B<sub>2</sub>O<sub>3</sub>," *J. Non-Cryst. Solids* **45**(1), 115–126 (1981), [http://dx.doi.org/10.1016/0022-3093\(81\)90096-X](http://dx.doi.org/10.1016/0022-3093(81)90096-X).

## Report Documentation Page

*Form Approved*  
*OMB No. 0704-0188*

Public reporting burden for the collection of information is estimated to average 1 hour per response, including the time for reviewing instructions, searching existing data sources, gathering and maintaining the data needed, and completing and reviewing the collection of information. Send comments regarding this burden estimate or any other aspect of this collection of information, including suggestions for reducing this burden, to Washington Headquarters Services, Directorate for Information Operations and Reports, 1215 Jefferson Davis Highway, Suite 1204, Arlington VA 22202-4302. Respondents should be aware that notwithstanding any other provision of law, no person shall be subject to a penalty for failing to comply with a collection of information if it does not display a currently valid OMB control number.

1. REPORT DATE <b>MAY 2011</b>	2. REPORT TYPE	3. DATES COVERED <b>00-00-2011 to 00-00-2011</b>		
4. TITLE AND SUBTITLE <b>Solid-core photonic bandgap fibers for cladding-pumped Raman amplification</b>		5a. CONTRACT NUMBER		
		5b. GRANT NUMBER		
		5c. PROGRAM ELEMENT NUMBER		
6. AUTHOR(S)		5d. PROJECT NUMBER		
		5e. TASK NUMBER		
		5f. WORK UNIT NUMBER		
7. PERFORMING ORGANIZATION NAME(S) AND ADDRESS(ES) <b>Air Command and Staff College, Air University, 225 Chennault Circle, Maxwell AFB, AL, 36112</b>		8. PERFORMING ORGANIZATION REPORT NUMBER		
9. SPONSORING/MONITORING AGENCY NAME(S) AND ADDRESS(ES)		10. SPONSOR/MONITOR'S ACRONYM(S)		
		11. SPONSOR/MONITOR'S REPORT NUMBER(S)		
12. DISTRIBUTION/AVAILABILITY STATEMENT <b>Approved for public release; distribution unlimited</b>				
13. SUPPLEMENTARY NOTES				
14. ABSTRACT <b>Cladding-pumped solid-core photonic bandgap Raman fiber amplifiers are analyzed theoretically as possible candidates for power scaling. An example fiber design with a mode field diameter of 46 μm and a cladding diameter of 250 μm is calculated to exhibit 0.12 dB/km of confinement loss at the first Stokes wavelength and &gt;10 dB/m at the second Stokes wavelength for a pump wavelength of 1.567 μm while maintaining low loss and large mode area in realistic coiling configurations. A Raman amplifier based on this fiber with 85 kW of output power, 78% optical conversion efficiency, a maximum heat load of 130 W/m, and a length of 235 m is simulated.</b>				
15. SUBJECT TERMS				
16. SECURITY CLASSIFICATION OF:			17. LIMITATION OF ABSTRACT	
a. REPORT <b>unclassified</b>	b. ABSTRACT <b>unclassified</b>	c. THIS PAGE <b>unclassified</b>	<b>Same as Report (SAR)</b>	18. NUMBER OF PAGES <b>15</b>
				19a. NAME OF RESPONSIBLE PERSON

12. Y. Jeong, S. Yoo, C. A. Codemard, J. Nilsson, J. K. Sahu, D. N. Payne, R. Horley, P. W. Turner, L. Hickey, A. Harker, M. Lovelady, and A. Piper, "Erbium:ytterbium codoped large-core fiber laser with 297-W continuous-wave output power," *IEEE J. Sel. Top. Quantum Electron.* **13**(3), 573–579 (2007), <http://dx.doi.org/10.1109/JSTQE.2007.897178>.
13. T. Miya, Y. Terunuma, T. Hosaka, and T. Miyashita, "Ultimate low-loss single-mode fibre at 1.55  $\mu\text{m}$ ," *Electron. Lett.* **15**(4), 106–108 (1979), <http://dx.doi.org/10.1049/el:19790077>.
14. S. D. Setzler, M. P. Francis, Y. E. Young, J. R. Konves, and E. P. Chicklis, "Resonantly pumped eyesafe erbium lasers," *IEEE J. Sel. Top. Quantum Electron.* **11**(3), 645–657 (2005), <http://dx.doi.org/10.1109/JSTQE.2005.850249>.
15. A. Shirakawa, H. Maruyama, K. Ueda, C. B. Olausson, J. K. Lyngsø, and J. Broeng, "High-power Yb-doped photonic bandgap fiber amplifier at 1150–1200 nm," *Opt. Express* **17**(2), 447–454 (2009), <http://www.opticsinfobase.org/oe/abstract.cfm?URI=oe-17-2-447>.
16. T. Muraö, K. Saitoh, and M. Koshiba, "Detailed theoretical investigation of bending properties in solid-core photonic bandgap fibers," *Opt. Express* **17**(9), 7615–7629 (2009), <http://www.opticsinfobase.org/oe/abstract.cfm?URI=oe-17-9-7615>.
17. W. Tong, H. Wei, J. Li, H. Wang, Q. Han, J. Luo, G. Ren, X. Yu, and P. Shum, "Investigation of all-solid photonic bandgap fiber with low losses in low-order bandgaps," *Opt. Quant. Electron.* **39**, 1071 (2008), <http://dx.doi.org/10.1007/s11082-007-9145-x>.
18. G. Bouwmans, L. Bigot, Y. Quiquempois, F. Lopez, L. Provino, and M. Douay, "Fabrication and characterization of an all-solid 2D photonic bandgap fiber with a low-loss region (< 20 dB/km) around 1550 nm," *Opt. Express* **13**(21), 8452–8459 (2005), <http://www.opticsinfobase.org/oe/abstract.cfm?URI=oe-13-21-8452>.
19. K. Tajima, J. Zhou, K. Nakajima, and K. Sato, "Ultralow loss and long length photonic crystal fiber," *J. Lightwave Technol.* **22**(1), 7–10 (2004), <http://dx.doi.org/10.1109/JLT.2003.822143>.
20. J. M. Fini, "Bend-resistant design of conventional and microstructure fibers with very large mode area," *Opt. Express* **14**(1), 69–81 (2006), <http://www.opticsinfobase.org/oe/abstract.cfm?URI=oe-14-1-69>.
21. A. Bétourné, G. Bouwmans, Y. Quiquempois, M. Perrin, and M. Douay, "Improvements of solid-core photonic bandgap fibers by means of interstitial air holes," *Opt. Lett.* **32**(12), 1719–1721 (2007), <http://www.opticsinfobase.org/abstract.cfm?URI=ol-32-12-1719>.
22. J. Bromage, K. Rottwitt, and M. E. Lines, "A method to predict the Raman gain spectra of germanosilicate fibers with arbitrary index profiles," *IEEE Photon. Technol. Lett.* **14**(1), 24–26 (2002), <http://dx.doi.org/10.1109/68.974149>.
23. C. Brooks, and F. Di Teodoro, "1-mJ energy, 1-MW peak-power, 10-W average-power, spectrally narrow, diffraction-limited pulses from a photonic-crystal fiber amplifier," *Opt. Express* **13**(22), 8999–9002 (2005), <http://www.opticsinfobase.org/abstract.cfm?URI=oe-13-22-8999>.
24. A. V. Smith, and B. T. Do, "Bulk and surface laser damage of silica by picosecond and nanosecond pulses at 1064 nm," *Appl. Opt.* **47**(26), 4812–4832 (2008), <http://www.opticsinfobase.org/abstract.cfm?URI=ao-47-26-4812>.
25. K. Petermann, and R. Kühne, "Upper and lower limits for the microbending loss in arbitrary single-mode fibers," *J. Lightwave Technol.* **4**(1), 2–7 (1986), <http://dx.doi.org/10.1109/JLT.1986.1074620>.
26. B. H. Bransden, and C. J. Joachain, *Introduction to Quantum Mechanics* (Wiley, 1989).
27. D. Marcuse, *Theory of Dielectric Optical Waveguides*. (Academic, 1991).
28. C. Jauregui, T. Eidam, J. Limpert, and A. Tünnermann, "The impact of modal interference on the beam quality of high-power fiber amplifiers," *Opt. Express* **19**(4), 3258–3271 (2011), <http://www.opticsinfobase.org/abstract.cfm?URI=oe-19-4-3258>.
29. B. Ward, and M. Mermelstein, "Modeling of inter-modal Brillouin gain in higher-order-mode fibers," *Opt. Express* **18**(3), 1952–1958 (2010), <http://www.opticsinfobase.org/oe/abstract.cfm?URI=oe-18-3-1952>.
30. S. L. Semjonov, O. N. Egorova, A. F. Kosolapov, A. E. Levchenko, V. V. Velmiskin, A. D. Pryamikov, M. Y. Salganskiy, V. F. Khopin, M. V. Yashkov, A. N. Guryanov, and E. M. Dianov, "LMA fibers based on two-dimensional solid-core photonic bandgap fiber design," *Proc. SPIE* **7580**, 758018, 758018-9 (2010), <http://dx.doi.org/10.1117/12.841265>.
31. M. Koshiba, and Y. Tsuji, "Curvilinear hybrid edge/nodal elements with triangular shape for guided-wave problems," *J. Lightwave Technol.* **18**(5), 737–743 (2000), <http://dx.doi.org/10.1109/50.842091>.
32. F. L. Teixeira, and W. C. Chew, "General closed-form pml constitutive tensors to match arbitrary bianisotropic and dispersive linear media," *IEEE Microwave Guided Wave Lett.* **8**, 223–225 (1998), <http://dx.doi.org/10.1109/75.678571>.
33. V. Hernandez, J. E. Roman, and V. Vidal, "SLEPC: A scalable and flexible toolkit for the solution of Eigenvalue problems," *ACM Trans. Math. Softw.* **31**(3), 351–362 (2005), <http://dx.doi.org/10.1109/75.678571>.
34. E. Coscelli, F. Poli, T. T. Alkeskjold, D. Passaro, A. Cucinotta, L. Leick, J. Broeng, and S. Selleri, "Single-mode analysis of Yb-doped double-cladding distributed spectral filtering photonic crystal fibers," *Opt. Express* **18**(26), 27197–27204 (2010), <http://www.opticsinfobase.org/abstract.cfm?URI=oe-18-26-27197>.
35. S. Johnson, and J. Joannopoulos, "Block-iterative frequency-domain methods for Maxwell's equations in a planewave basis," *Opt. Express* **8**(3), 173–190 (2001), <http://www.opticsinfobase.org/oe/abstract.cfm?URI=oe-8-3-173>.
36. R. T. Schermer, and J. H. Cole, "Improved bend loss formula verified for Optical Fiber by simulation and experiment," *IEEE J. Quantum Electron.* **43**(10), 899–909 (2007), <http://dx.doi.org/10.1109/JQE.2007.903364>.

37. M. H. Muendel, R. Farrow, K. Liao, D. Woll, J. Luu, C. Zhang, J. J. Morehead, J. Segall, J. Gregg, K. Tai, B. Kharlamov, H. Yu, and L. Myers, "Fused fiber pump and signal combiners for a 4-kW ytterbium fiber laser," Proc. SPIE **7914**, 791431, 791431-7 (2011), <http://dx.doi.org/10.1117/12.877572>.
  38. D. C. Brown, and H. J. Hoffman, "Thermal, stress, and thermo-optic effects in high average power double-clad silica fiber lasers," IEEE J. Quant. Electron. **37**, 207–217 (2001), <http://dx.doi.org/10.1109/3.903070>.
  39. G. P. Agrawal, *Nonlinear Fiber Optics*, 3rd ed. (Academic Press, 2001).
  40. L. B. Glebov, "Intrinsic laser-induced breakdown of silicate glasses," Proc. SPIE **4679**, 321–331 (2002), <http://dx.doi.org/10.1117/12.461727>.
  41. J. C. Travers, A. B. Rulkov, B. A. Cumberland, S. V. Popov, and J. R. Taylor, "Visible supercontinuum generation in photonic crystal fibers with a 400 W continuous wave fiber laser," Opt. Express **16**(19), 14435–14447 (2008), <http://www.opticsinfobase.org/oe/abstract.cfm?URI=oe-16-19-14435>.
- 

## 1. Introduction

Recently an upper limit of ~40 kW has been proposed for the average power achievable using double-clad fiber lasers under a set of reasonable assumptions [1]. The power was found to be limited by thermal lensing and stimulated Raman scattering (SRS) regardless of the achievable mode field area. Solutions mitigating these limits would in theory enable further power scaling.

W-type, dual-hole assisted, and solid-core photonic bandgap fibers (SCPBGF) have been investigated as possible means to increase the SRS threshold in fibers [2–4]. Of these approaches, SCPBGF have enabled the largest mode field area of 413  $\mu\text{m}^2$  [4] compared to 155  $\mu\text{m}^2$  for a proposed w-type fiber [2] and 78  $\mu\text{m}^2$  for the dual hole-assisted fiber [3]. Optimization of w-type fiber designs for SRS suppression depends on balancing mode field area against spectral filtering cutoff sharpness [2]. In contrast, core size does not affect the spectral filtering cutoff properties of PBGF which are rather determined by the resonance properties of high index inclusions comprising the cladding structure [5]. Therefore SCPBGF represent an opportunity for mode field area scaling in SRS-suppressing fibers.

Mitigation of thermal lensing has received less attention due to its relative unimportance so far. One proposed approach has been to depress the core refractive index in a photonic crystal fiber relative to the cladding so that the thermal lens causes the core index to approach that of the cladding at high thermal loads [6]. In order to reach the thermal lens and SRS limits, a mode field diameter of 90  $\mu\text{m}$  was determined necessary [1]. Single transverse mode operation is difficult to achieve for mode field diameters this large. One of the main reasons is that it is difficult to achieve a highly uniform refractive index profile in a doped core [1]. Minimum index variations on the order of  $10^{-4}$  achievable with state-of-the-art manufacturing methods [7] cannot ensure the stability of the fundamental mode in such large cores.

Raman fiber amplifiers (RFA), in contrast, do not require doped cores. While core-pumped Raman fiber amplifiers are useful for generating wavelengths inaccessible with rare earth fibers, they offer no increase in brightness beyond that of the pump source unless pumped from both ends in which case a modest brightness gain of less than 2 is possible. Cladding-pumped Raman fiber amplifiers (CPRFA) do however enable an increase in brightness [8–10]. CPRFA rely on a dual-waveguide structure wherein the Raman pump propagates in the outer waveguide, or pump cladding, while the Stokes is amplified within the inner waveguide, or core. The brightness gain advantage of CPRFA over core-pumped RFA arises from the ability to couple more pump power to the larger pump cladding which also typically has a high numerical aperture.

The growth of the second Stokes wave, which is seeded by noise and core-pumped, limits the brightness enhancement as well as the total amount of pump power that can be converted into the first Stokes wave [8–10]. One method of extending the brightness enhancement limit is to employ a fiber design that exhibits high loss at the second Stokes wavelength and low loss at the first Stokes wavelength [9,10]. However, this approach is subject to the same tradeoffs between mode field area and induced Stokes loss as rare earth doped SRS suppressing fibers. One additional benefit of CPRFA is that they require very long fiber lengths therefore they create a modest heat load even for very high average powers thus mitigating thermal lensing [10].

This work argues that solid-core photonic bandgap fibers with low loss at the first Stokes wavelength and very high loss at the second Stokes wavelength can enable power scaling of cladding-pumped Raman fiber lasers and amplifiers as proposed previously [8]. General considerations of this approach are discussed and then a candidate SCPBGF design is analyzed theoretically and evaluated with respect to its anticipated capabilities and usefulness in a CPRFA.

## 2. General considerations

Desired characteristics of fiber sources include high power, high efficiency and good beam quality. The optical conversion efficiency of a CPRFA is determined by pump and Stokes material and waveguide losses and completeness of pump conversion [8,9]. For sufficiently strong second Stokes suppression, long fibers enable a large fraction of the pump to be converted to the first Stokes wavelength [8–10]. The present study is focused on fibers with a pump wavelength of 1.567  $\mu\text{m}$  with first and second Stokes wavelengths of 1.683  $\mu\text{m}$  and 1.818  $\mu\text{m}$  respectively based on the Raman wavenumber shift of 440  $\text{cm}^{-1}$  for fused silica [11] and the signal wavelength of a reported high-power Er-Yb fiber source [12]. Fused silica fibers exhibit the lowest material loss in the telecommunications band near 1.550  $\mu\text{m}$  [13]. These wavelengths also present a reduced risk of eye injury [14].

The maximum pump power that can be launched into the fiber cladding is a function of the pump source brightness and the diameter and numerical aperture of the pump cladding. Diode-pumped double-clad rare earth fiber lasers are attractive candidates for pump sources. The power that can be coupled from multiple single transverse mode (STM) fiber sources into a multi-mode pump cladding may be derived by considering the divergence angle of the freely propagating output of a STM fiber. Brightness conversion then limits the pumping power to

$$P_{\text{cl}} \leq \left( \frac{\pi d_{\text{cl}} NA_{\text{cl}}}{2\lambda} \right)^2 P_p, \quad (1)$$

where  $d_{\text{cl}}$  and  $NA_{\text{cl}}$  are the diameter and numerical aperture of the pump cladding,  $\lambda$  is the pump wavelength, and  $P_p$  is the power available from each STM fiber pump source. It is important to realize that this expression does not assume coherent combination of the STM fiber sources. If the Raman amplification process converts this power to a STM Stokes beam with conversion efficiency  $\eta_c$  then the brightness enhancement is limited to  $B \leq \eta_c (\pi d_{\text{cl}} NA_{\text{cl}} / 2\lambda)^2$  as shown previously [9].

In SCPBGF used in CPRFA not all of the power launched into the cladding is available for Raman pumping. Some pump light is confined to modes guided in the high index cladding structure that have poor overlap with the core region. The fraction of trapped light increases as the total area and refractive index of all high index cladding features increases. Assuming that the cladding is uniformly-pumped at its maximum numerical aperture and that the photonic band gap (PBG) structure comprised of a triangular array of cylindrical inclusions occupies the majority of the pump cladding results in the following expression for a lower limit for the pump injection efficiency:

$$\eta_p \geq 1 - \frac{N_i A_i}{A_{\text{cl}}} \frac{NA_i^2}{NA_{\text{cl}}^2} = 1 - \frac{\pi}{\sqrt{3}} \left( \frac{d}{\Lambda} \right)^2 \frac{n\Delta n}{NA_{\text{cl}}^2}, \quad (2)$$

where  $N_i$  is the number of inclusions,  $A_i$  is the area occupied by one inclusion,  $NA_i$  is the numerical aperture of the inclusions,  $A_{\text{cl}}$  is the cladding area,  $d$  is the inclusion diameter,  $\Lambda$  is the lattice pitch,  $n$  is the background refractive index,  $\Delta n$  is the index step of the inclusions, and  $NA_{\text{cl}}$  is the numerical aperture of the pump cladding. This expression predicts the pump efficiency to be at least 78% for the cladding-pumped Yb-doped PBGF described in [15] while 88% was observed. The better efficiency is attributable to the pump cladding region

beyond the PBG structure. In this case, the high pump cladding numerical aperture significantly enhances the efficiency.

To achieve high efficiency, the signal core of the fiber must exhibit low signal loss at the first Stokes wavelength. Waveguide confinement loss and material loss contribute to the total loss. Although theoretical confinement losses below  $10^{-5}$  dB/km have been reported for SCPBGF [16], the best experimental result to date has been 2 dB/km at 1.310  $\mu\text{m}$  [17] of which 1.2 dB/km was attributed to material losses due to water contamination. It is believed that improvements in the manufacturing process can decrease the loss further [17]. Low-loss fibers have also incorporated graded index (GRIN) high index regions [17,18]. Improvements in the manufacturing process of index guiding photonic crystal fibers have decreased experimentally observed loss to 0.37 dB/km near 1.550  $\mu\text{m}$  [19]. One of the keys to low loss in these fibers is the minimization of surface roughness at the boundaries of the air holes. This suggests that GRIN inclusions in SCPBGF may help decrease loss by minimizing roughness at the inclusion boundaries. An additional benefit of employing parabolic GRIN inclusions is that they enable highly reduced bend-induced mode field distortion within each inclusion [20] thus rendering the cladding photonic band structure more stable overall against bending.

One prerequisite for low confinement loss in SCPBGF is adequate cladding thickness [16]. Increasing the thickness of the cladding decreases the pump intensity for a given pump brightness however. Furthermore, it necessitates a larger pump cladding thus placing a more stringent high loss requirement on the second Stokes [10]. The depth and order of the chosen bandgap also influences the confinement loss. Signals guided in higher-order bandgaps exhibit lower loss [16]. For high order bandgaps to exist in the cladding, the inclusions forming the PBG structure must support a large number of guided modes which requires that they have relatively high numerical aperture and large diameter. Another method of decreasing loss is to introduce air holes into the PBG structure [21]. Considering these factors, it is reasonable to expect that a loss of 1 dB/km for a SCPBGF operating further into the infrared material loss regime at 1.683  $\mu\text{m}$  is possible. This was also the loss value assumed in a recent theoretical analysis of CPRFLs employing a w-type fiber [9].

The possibility that the PBG cladding structure would exhibit SRS thus depleting the pump and decreasing efficiency also requires attention. The array of cylindrical high index inclusions may be thought of as a multi-core fiber that can exhibit amplification of noise through the Raman process. This can compete with the amplification of the desired signal. This situation is exacerbated by the fact that germanosilicate glass typically used to form the high-index inclusions generally exhibits a significantly higher Raman gain coefficient than pure fused silica [22].

Although SCPBGF-based CPRFA can mitigate SRS and thermal lensing, the bulk damage threshold may still limit the achievable output power. Although a maximum average intensity of  $10 \text{ W}/\mu\text{m}^2$  was assumed in a previous analysis of fiber laser power scaling [9], almost  $2 \text{ kW}/\mu\text{m}^2$  has been demonstrated in a fiber source with  $\sim 1$  ns pulse duration [23]. This is consistent with recent bulk damage threshold measurements in silica [24]. This suggests that a slow-onset process such as heating would ultimately be responsible for bulk damage.

Fibers with increasingly large core diameters support increasing numbers of guided modes that are detrimental to output beam quality. Furthermore, they become affected by bend-induced mode distortion [20]. Also, unintended variations in the core refractive index of doped fibers limit the degree to which the profile may be manipulated to reduce the number of guided modes [1]. It is important to understand how removing this last limitation can affect the capabilities of SCPBGF-based CPRFL. One method of improving the beam quality of few-moded fibers is to attempt to induce preferential loss in the higher order modes. Alternatively an input beam may be matched to the fundamental mode of the core and steps taken to reduce coupling into other guided modes.

One of the primary causes of mode coupling in large-core fibers is bend-induced effective refractive index profile change. This mechanism has been studied extensively in the context of microbend losses in single-mode fibers [25]. If the variation of the curvature radius is gradual enough, then the adiabatic approximation applies and mode coupling will be absent. The

conditions under which this is the case may be found by solving the scalar paraxial wave equation

$$\begin{aligned} i \frac{\partial \psi}{\partial z} &= \frac{1}{2\beta} \left[ \nabla_t^2 + \left( n(x, y)^2 k_0^2 - \beta^2 \right) \right] \psi \\ &= \frac{1}{2\beta} \left[ \nabla_t^2 + \left( \left( n_0(x, y) + \Delta n(x, y) \right)^2 k_0^2 - \beta^2 \right) \right] \psi, \end{aligned} \quad (3)$$

in the limit that the refractive index profile varies gradually along the fiber. In Eq. (3),  $\psi$  is a function of position and represents the slowly-varying envelope of the electric field within the fiber,  $\beta$  is a chosen propagation constant,  $k_0 = \omega/c$  is the propagation constant in a vacuum, and  $n(x, y)$  is the refractive index profile. This equation is analogous to the time dependent Schrödinger equation with time being replaced by propagation distance and the value of  $\hbar$  being set to 1. The detailed procedure for deriving the adiabatic limit is described elsewhere [26]. Restricting the system to two transverse modes, the adiabatic condition thus arrived at is

$$\left| \frac{\beta_i}{(\beta_i - \beta_j)^2} \langle \phi_i | x | \phi_j \rangle \frac{d}{dz} \left( \frac{1}{R} \right) \right| \ll 1, \quad (4)$$

where  $\beta_i$  and  $\beta_j$  are the propagation constants of the two modes,  $\phi_i$  and  $\phi_j$  are their normalized field profiles in the scalar approximation, the angular brackets represent integration over the fiber cross-section,  $R$  is the effective radius of curvature,  $z$  is the axis of propagation, and the effective index profile

$$n(x, y) = n_0(x, y) \left( 1 + \frac{x}{R} \right) \quad (5)$$

has been assumed [16,27,36]. It is evident from Eq. (3) and (5) that the role of the time dependent part of the quantum mechanical Hamiltonian operator is represented in the present case by

$$\delta H(x, y, z) \equiv \left( \frac{n_0^2(x, y) k_0^2}{\beta} \right) \left( \frac{x}{R(z)} \right) \approx \frac{\beta x}{R(z)}. \quad (6)$$

Equation (4) may be simplified considerably if the two modes are assumed to be LP<sub>01</sub> and LP<sub>11</sub> in which case the term with the integral may be approximated roughly by the diameter  $a$  of the fiber core. Furthermore, assuming that the two values of  $\beta$  are separated by a small value  $\Delta\beta = (2\pi/\lambda)\Delta n_{\text{eff}}$ , where  $n_{\text{eff}}$  is the effective index, the adiabatic condition becomes

$$\left| \frac{d}{dz} \left( \frac{1}{R} \right) \right| \ll \frac{2\pi\Delta n_{\text{eff}}^2}{n_{\text{eff}} a \lambda}. \quad (7)$$

If the fiber can be maintained in a configuration satisfying Eq. (7), then it is reasonable to expect that it may be free from bending induced mode coupling.

Another cause of mode coupling is modal interference [28]. In this case, the quantum mechanical analog of the fiber is a two-level system under the influence of a resonant harmonic perturbation. Therefore the paraxial spatial frequency at which power is transferred through modal coupling in the fiber is analogous to the Rabi oscillation frequency [26]. In this

case, modal interference causes a change in local refractive index along the fiber that may be approximated using the interference term between the two modes being coupled yielding

$$\Delta n(x, y, z) = \Delta n_0 A_c \phi_i(x, y) \phi_j(x, y) \sin[(\beta_i - \beta_j)z], \quad (8)$$

where the constant  $\Delta n_0$  represents the maximum amplitude of local refractive index change which depends on the signal power, the distribution of power between the modes, and the modulation mechanism. The exact functional form relating the interference term to the refractive index change also depends on the modulation mechanism [28]. In the present case this would most likely be thermal refractive index change. Also the factor  $A_c$  is the area within the core in which the refractive index change occurs such that

$$\frac{1}{A_c} \equiv \max_{(x,y)} [\phi_i(x, y) \phi_j(x, y)]. \quad (9)$$

This definition of  $A_c$  causes the maximum local amplitude of  $\Delta n$  to be  $\Delta n_0$ . The units are area due to the normalization of the field profiles. Invoking the rotating wave approximation [26], valid because the modal beating occurs on a length scale much shorter than the transfer length  $L_T$ , reduces Eq. (3) to a set of linear coupled differential equations describing power transfer back and forth between the two transverse modes [26] with a spatial period or transfer length of

$$L_T = \frac{2\pi}{\beta_T} = \frac{2\lambda A_{ij}}{\Delta n_0 A_c}, \quad (10)$$

where  $A_{ij}$  is the effective inter-modal area [29] and  $\beta_T$  is the paraxial analog of the Rabi frequency [26]. Equation (10) could also be derived using coupled mode theory [27]. Applying this equation to a situation similar to a fiber amplifier previously studied [28] with a core diameter of 80  $\mu\text{m}$  operating at 1.064  $\mu\text{m}$  yields the values  $\Delta n_0 \approx 4 \times 10^{-6}$ ,  $A_{12} = 6200 \mu\text{m}^2$ ,  $A_c = 3000 \mu\text{m}^2$  for coupling between the  $\text{LP}_{01}$  and  $\text{LP}_{11}$  modes. These values yield a mode transfer length of 1.1 m in good qualitative agreement with, although somewhat shorter than, the previously reported result [28]. The approximate treatment presented here neglects confinement of the doped region to the center of the core furthermore it does not account for the changing power in the two modes. It can be useful however in predicting when this source of coupling may be an issue.

One interesting observation regarding the two types of modal coupling discussed above is that large effective index spacing between modes mitigates bending induced mode coupling but not coupling caused by interference. In light of these general observations, a specific candidate fiber design is now considered.

### 3. Fiber design

Given that a relatively sharp increase in loss with wavelength is required to achieve simultaneously low first Stokes loss and high second Stokes loss the third bandgap was chosen to guide the first Stokes. While higher order bandgaps are more susceptible to bending-induced loss variability this is less of an issue for laser fibers that can be arranged deliberately to control the bending radius along the length in contrast to telecommunications fibers that must tolerate a range of configurations. Based on prior reported results [16–18] it is evident that a  $\Delta n$  value of  $\sim 0.03$  and an inclusion diameter  $d$  of  $\sim 10 \mu\text{m}$  will place a pure silica core defect mode in the 3rd bandgap at a 1.683  $\mu\text{m}$  wavelength.

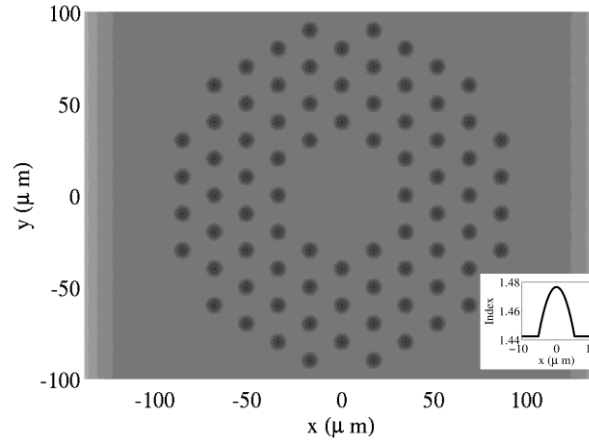


Fig. 1. Solid-core photonic bandgap fiber incorporating parabolic graded-index inclusions. Darker regions represent higher refractive index. The inset shows the index profile of each inclusion.

Furthermore, the candidate design incorporates GRIN inclusions arranged in a triangular lattice. The maximum index increase over background is 0.0342 and the diameter of the doped regions is 10.4  $\mu\text{m}$ . The lattice pitch is 20  $\mu\text{m}$  resulting in a diameter to pitch ratio of 0.52. The central core is formed by the omission of 7 inclusions. While this causes multiple transverse modes to be guided, the alternative of shrinking the core would reduce the maximum output power due to the bulk optical damage threshold while increasing the pitch would lead to an unacceptable amount of confinement loss [30]. Therefore this design is not inherently single-mode and effectively single-mode operation may or may not be possible. The cladding incorporates three complete rings of defects and one incomplete ring to better fit within a uniform diameter pump cladding. Figure 1 depicts the fiber cross section.

This design was optimized for loss at the second Stokes wavelength of 1.818  $\mu\text{m}$  by varying the maximum index increase and calculating confinement loss using a fully-vectorial finite element method based on curvilinear linear tangential, quadratic nodal hybrid elements with perfectly matched layer boundary conditions [31,32] to construct the finite element matrices  $\mathbf{K}$  and  $\mathbf{M}$  defining the generalized eigenproblem

$$(\mathbf{K} - \beta^2 \mathbf{M})\phi = 0. \quad (11)$$

In this equation  $\beta$  is the propagation constant and  $\phi$  is the finite element state vector defining the nodal and tangential electric field values. The confinement losses were then calculated from  $\beta$ . A structured mesh preserving the symmetry of the fiber with uniform density across the entire integration domain was used. Equation (11) was then solved using a freely-available parallel computational library for the solution of large sparse eigenproblems [33]. The effective modal index of the core and the confinement loss as a function of wavelength are shown in Fig. 2. At the target first Stokes wavelength of 1.683  $\mu\text{m}$ , the confinement loss is  $1.2 \times 10^{-4}$  dB/m while within a range of wavelengths spanning 17 nm near the second Stokes gain peak the loss is approximately 10 dB/m. The non-linear effective area of the fundamental mode is 1670  $\mu\text{m}^2$  with a mode field diameter of 46  $\mu\text{m}$ . Although the range of wavelengths at which suppression occurs does not span the entire range between the first and second Stokes gain peaks, incorporating heterogeneous inclusions in the fiber cladding has been shown to enable combining the filtering properties of each of the inclusion types [34]. Applications requiring suppression of this entire wavelength range call for further investigations of SCPBGF with an appropriate spread of inclusion sizes.

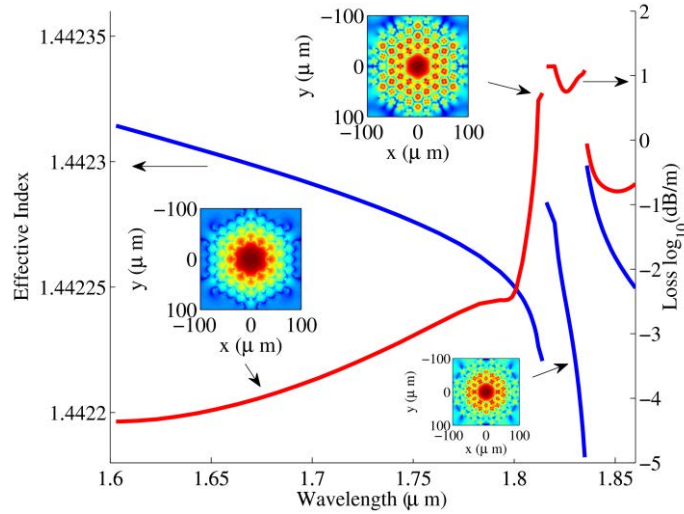


Fig. 2. Plots of the calculated effective index and confinement loss of the fundamental mode of the fiber as a function of wavelength. Insets depict the logarithmic intensity profile at the signal wavelength of 1.683  $\mu\text{m}$  and the wavelengths 1.814  $\mu\text{m}$  and 1.826  $\mu\text{m}$  near the upper band edge.

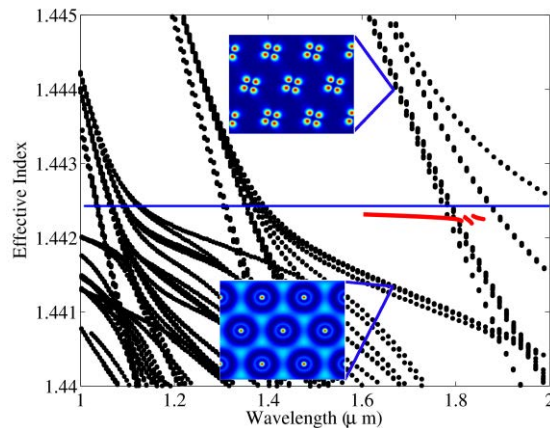


Fig. 3. Photonic band structure of the candidate fiber design sampled at a discrete set of wave vectors describing the Bloch states of the periodic lattice. The blue line represents the index of the silica background at 1.683  $\mu\text{m}$  and the red line represents the index of the fundamental guided core mode at wavelengths spanning 1.6  $\mu\text{m}$  - 1.86  $\mu\text{m}$ . The insets depict the intensity profiles of the cladding modes bounding the guided mode.

To facilitate comparison with a prior related publication [16], the material dispersion contribution was subtracted from the effective index values. The rapid increase in loss near the band edge is particularly significant and effectively serves as a cutoff wavelength for the second Stokes. The wavelength of this cutoff can be controlled by scaling the geometry of the fiber structure. The ideal wavelength will depend on the bandwidth of the first Stokes signal. For narrow signals, the cutoff should be at a higher wavelength to minimize the first Stokes loss. For broad signals, the cutoff should be at a lower wavelength to create loss across a significant portion of the Raman gain spectrum near the second Stokes wavelength. The jumps in effective index near the wavelengths of 1.818  $\mu\text{m}$  and 1.835  $\mu\text{m}$  suggest that the mode is guided in successively lower order bandgaps above these wavelengths.

To analyze the photonic band structure of the PBG cladding, fully-vectorial eigenmodes of Maxwell's equations with periodic boundary conditions were computed by preconditioned

conjugate-gradient minimization of the block Rayleigh quotient in a planewave basis, using a freely available software package [35]. Figure 3 shows the relationship between the effective index of the guided fundamental mode and the cladding modes for a range of wavelengths. The band structure thus obtained confirms that the loss increases as the fundamental guided core mode approaches the band edge. The high losses at wavelengths beyond 1.820  $\mu\text{m}$  occur as the mode is guided in a minor gap within the band between the second and third primary band gaps. The discontinuity in the effective index occurs at the red edge of the band.

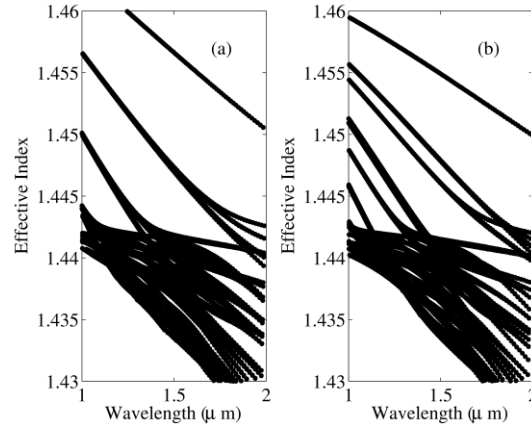


Fig. 4. Calculated band structure for triangular lattices of parabolic GRIN inclusions (a) and step-index inclusions (b). The properties of the GRIN inclusions match those of the SCPBGF described above. The properties of the step-index inclusions were chosen to place the red edge of the third band-gap at approximately the same place as the GRIN-based fiber.

At wavelengths beyond 1.840  $\mu\text{m}$  the core and cladding modes are approximately degenerate rendering core mode loss an ill-defined quantity. The upper and lower numerical apertures relative to the cladding mode indices [30] at 1.683  $\mu\text{m}$  are 0.066 and 0.054 respectively yielding  $V$  parameters of 5.7 and 4.6 confirming that the fiber is multi-mode. Evaluating Eq. (7) yields an adiabatic mode coupling limit of 2250  $\text{m}^{-2}$  on the radius of curvature change rate for this fiber.

It is interesting to compare the photonic band structure of the GRIN-type SCPBGF to that of a SCPBGF with step-index (SI) inclusions. Figure 4 shows the band structure in the neighborhood of the third bandgap for fibers of each type. The gaps for the SI-type fiber are not as broad and the bands are broader relative to the GRIN-type fiber. This demonstrates that inclusions with approximately the same diameter and index step can exhibit significantly different band structure leading to different guiding properties. A comprehensive comparison between SI-type and GRIN-type SCPBGF, though perhaps warranted, is outside the scope of this paper.

The fiber must be coiled to some reasonable diameter for use in a practical device. The two primary concerns for coiling large-mode-area fibers are excessive fundamental mode bend loss that causes low efficiency and mode field distortion that reduces the effective area thus lowering the power handling capacity. The bend-induced confinement loss increase and mode field area decrease were investigated using the finite element scheme discussed above.

One previously discussed method of treating the effects of coiling is to employ the equivalent straight waveguide (ESW) approximation [16,36]. In the calculations presented here, the refractive index tensor is modified due to coiling-induced stress, and the absorbing boundary conditions. Therefore it is found more convenient to keep the original index profile, modify the trial solution to describe propagation in a curved fiber

$$\vec{E}(x, y, z, t) = \vec{f}(x, y) \exp \left[ -i \left( \beta \left[ 1 + \frac{x}{R} \right] z - \omega t \right) \right] \quad (12)$$

and employ the finite element method to solve for the field profile at  $z = 0$ . The validity of this procedure stems from the fact that no modification of the optical wave equation occurs due to the substitution specified by Eq. (12), the observation that this functional form maintains the orientation of the optical phase relative to the curved fiber, and the local nature of the optical wave equation. This method for calculating the bending loss also does not require further artificial manipulation of the effective index profile beyond the caustic radius [36]. Furthermore, it has also been verified against published experimental and theoretical results for bending losses in step index fibers [36].

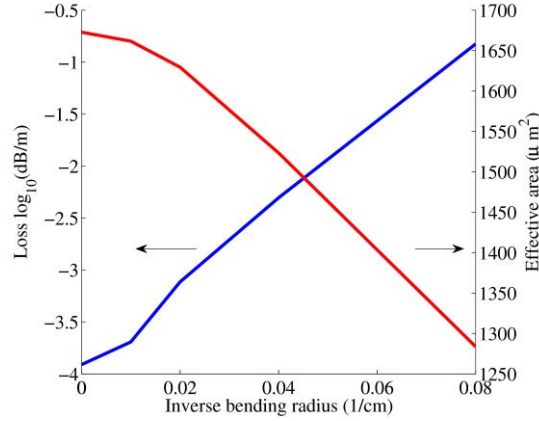


Fig. 5. Confinement loss and effective area as a function of inverse bending radius at 1.683  $\mu\text{m}$  wavelength.

Figure 5 shows the bend-induced confinement loss and mode field area as a function of inverse bending radius. It is evident that larger coils are beneficial for both power and efficiency. The maximum tolerable coil diameter will then be restricted by packaging considerations. If a 2 meter diameter is acceptable, then the mode field area will be reduced by less than 1% while the confinement loss will increase to only 0.2 dB/km. The loss near the second Stokes wavelength also increases with bending.

The inner-cladding should be as small as possible to provide maximum pumping intensity for a given available pump power. The size is limited by the requirement for this cladding to accommodate the PBG structure. The diameter of the PBG structure is approximately 200  $\mu\text{m}$  as shown in Fig. 1 therefore a pump clad diameter of 250  $\mu\text{m}$  is sufficient to contain the entire structure leaving some room to ease the fabrication process. A fluorosilicate glass outer cladding is assumed resulting in a pumping numerical aperture of 0.30. In summary, the proposed fiber has a core diameter of 46  $\mu\text{m}$  with a 0.054 numerical aperture and a pump cladding of diameter 250  $\mu\text{m}$  with a 0.30 numerical aperture.

#### 4. Amplifier simulation

A SCPBGF CPRFA incorporating the fiber described above in a co-pumped configuration is considered. The coupled set of differential equations describing this system is [8]

$$\frac{dP_p}{dz} = -\alpha_p P_p - \frac{g_0 \lambda_{s1}}{A_{cl} \lambda_p} P_p P_{s1} - \frac{g_1 \lambda_{s1c}}{A_{cl} \lambda_p} P_p P_{s1c}, \quad (13a)$$

$$\frac{dP_{s1}}{dz} = -\alpha_{s1} P_{s1} + \frac{g_0}{A_{cl}} P_{s1} P_p - \frac{g_0 \lambda_{s2}}{A_{co} \lambda_{s1}} P_{s1} P_{s2}, \quad (13b)$$

$$\frac{dP_{s1c}}{dz} = -\alpha_{s1c} P_{s1c} + \frac{g_1}{A_{cl}} P_{s1c} P_p, \quad (13c)$$

$$\frac{dP_{s2}}{dz} = -\alpha_{s2} P_{s2} + \frac{g_0}{A_{co}} P_{s2} P_{s1}. \quad (13d)$$

In these equations,  $P$  denotes power,  $z$  is propagation distance,  $\alpha$  is loss,  $g_0$  is the Raman gain coefficient in pure silica,  $g_1$  is the Raman gain coefficient in the germanosilicate inclusions,  $A$  is area, and  $\lambda$  is wavelength. The subscript p denotes the Raman pump, s1 the first Stokes signal in the core, s1c the first Stokes signal in the inclusions, s2 the second Stokes signal in the core. The subscripts cl and co refer to the cladding and the core respectively. The pump and first Stokes signal are assumed to be launched with a given power in the cladding and core respectively while the second Stokes in the core and the first Stokes in the inclusions build up from noise. The effective seed power in this case is taken to be the product of the energy of one Stokes photon and the Raman gain bandwidth [39]. The bandwidth of the seed source is assumed to be broad enough that stimulated Brillouin scattering does not affect the operation of the amplifier. Finally counter-pumped Stokes waves are neglected as discussed below.

One prominent feature of the fiber discussed here is that to accommodate the guiding structure, the pump cladding diameter must be approximately 250  $\mu\text{m}$ . This large value reduces the pump intensity. This leads to long fibers or high required pump powers. Additionally, the length of large diameter fiber that can be manufactured within tolerance from a single pre-form is limited. In one case, a 387 meter long draw was achieved [18]. A practical fiber length limit of 500 meters is assumed here. The effective Raman gain coefficient in the core is taken to be  $3.2 \times 10^{-14}$  m/W based on scaling the value at a 1  $\mu\text{m}$  wavelength [39] for the pump wavelength of 1.567  $\mu\text{m}$  and the un-polarized pump (factor of 0.5 [39]). The Raman gain coefficient in the cladding inclusions is taken to be  $6.3 \times 10^{-14}$  m/W based on a prior reported value [8]. Furthermore, the modes within the inclusions are well confined so that their amplification is governed only by this second Raman gain coefficient. The total confinement and material loss within the core at 1.683  $\mu\text{m}$  is 1 dB/km while at 1.818  $\mu\text{m}$  it is 10 dB/m based on the finite element calculations. Pump loss is 2 dB/km and loss for the fundamental mode guiding in the cladding structure is 0.2 dB/km. The first Stokes in the inclusions is shifted by 425  $\text{cm}^{-1}$  from the pump resulting in a 1.679  $\mu\text{m}$  wavelength. A seed power of 10 W provided by a core-pumped fiber Raman oscillator is presumed. Additionally, fundamental mode propagation within the core is assumed.

Equation (13a)-(13d) were solved using a Runge-Kutta numerical method for a range of launched pump powers. The results are summarized in Fig. 6. According to these calculations, the launched pump power must be several tens of kilowatts in order to obtain good efficiency. A scheme for combining 637 individual pump sources using fused fiber bundles has been reported [37]. To reach 50 kW of total pump power, such a scheme would require 79 W from each source. While this would be very challenging to accomplish with single-emitter diode pump sources it is relatively easy to achieve with STM fiber lasers. If 100 W were available from a STM pump source, then brightness conservation would limit the maximum available pump power to 565 kW according to Eq. (1); however, this would require the combination of 5,650 individual sources. Combining such a large number of fibers may prove to be impractical, in which case the engineering of fused fiber combiners would determine the true limit.

As the pumping power is increased the maximum heat load increases as well. The maximum heating occurs along the fiber where the pump is being depleted most rapidly. In the absence of sufficient seed power, spontaneous Raman scattering is amplified in the cladding structure first by virtue of its higher Raman gain coefficient thus depleting the pump and preventing amplification in the core.

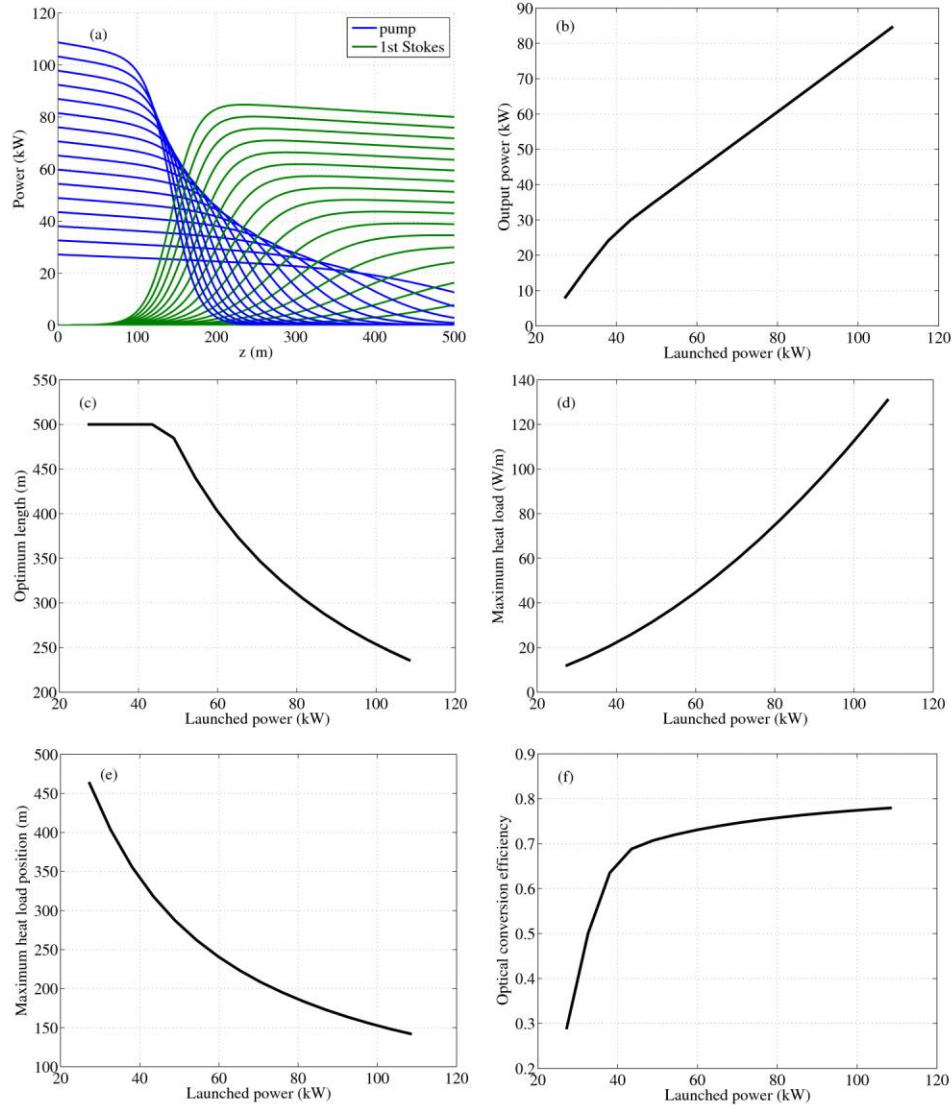


Fig. 6. Simulation results for a SCPBGF CPRFA including the evolution of pump and signal over the length of the fiber (a), peak first Stokes power (b), optimum fiber length (c), maximum heat load (d), location along the fiber of the maximum heat load (e), and optical conversion efficiency (f). All results take into account the trapping of 8% of the pump power within the cladding structure.

Furthermore, the high loss at the second Stokes wavelength enabled the by the SCPBGF completely suppresses amplification at this wavelength. At the highest launched pump power, the first Stokes power in the inclusions that has built up from noise is calculated to be 265 W representing a small fraction of the total output power. The counter-propagating first Stokes power in the inclusions is even weaker due to the much lower pump power at the output end of the fibers therefore it is omitted in the solutions of Eq. (13a)-(13d).

Typically a shooting algorithm would be used to treat the counter-propagating second Stokes [9] seeded by spontaneous Raman scattering. In the present case however, the suppression of the second Stokes by the fiber is so strong that the counter-propagating Stokes field is so weak at the pumped end of the fiber that its representation in the computer program would be below the minimum double precision real value. Rather, the worst case scenario of

the second Stokes being pumped by the full output value of the first Stokes was considered to see if the second Stokes can be amplified. Using Eq. (13d) this condition may be expressed

$$\alpha_{s_2} > \frac{g_0 P_{s1}(L)}{A_{c_0}}. \quad (14)$$

Evaluating this at the maximum calculated output power of 85 kW yielded 7 dB/m of required second Stokes attenuation.

For such high pump powers, heating of the fiber can become an issue even for such long fibers. An upper limit on the heat generated in the fiber is given by the total optical power lost per unit length from the four signals described by Eq. (13a)-(13d). The maximum value and the position along the fiber at which this maximum occurs are shown in Fig. 6(d) and Fig. 6(e). The heating obtained by this method overestimates the true deposited heat because it assumes all loss is converted to heat while some signal loss, such as confinement loss and Rayleigh scattering, transfers power optically.

It is also important to consider possible temperature-induced radial refractive index profile perturbations within the inclusions due to additional absorption caused by the varying germanium doping level. The doping adds approximately 0.1 dB/km of additional loss over pure silica. For 110 kW of pump power evenly distributed throughout the pump cladding, this amounts to 0.004 W/m of additional heat load in each inclusion. Comparison to a prior thermal study of fiber lasers indicates that the index profile perturbation due to this heat load is negligible [38]. Quantum defect heating caused by Raman process concentrates the heat load in the core. In this case, the temperature profile assumes a maximum value in the center of the core and decays rapidly within the core heating region and then more gradually throughout the cladding [38]. The predicted maximum heating of 130 W/m is far below a previously reported thermal lensing threshold [1].

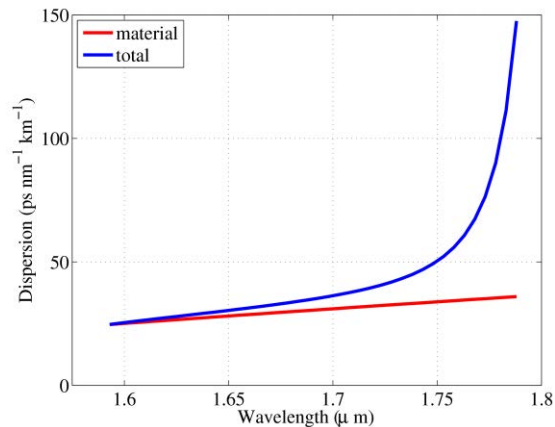


Fig. 7. Calculated material and total dispersion for the fundamental core mode of the fiber.

The temperature induced refractive index change may be enough to induce coupling to the LP<sub>11</sub> mode through the modal interference mechanism. In this case, the broad signal spectrum as well as the temporal fluctuations typical of such spectra may degrade or destroy the interference. The maximum optical power density at 85 kW of first Stokes continuous-wave (CW) power in the core is 51 W/μm<sup>2</sup>. The author is not aware of any results in the literature for the CW optical damage threshold of pure fused silica for wavelengths near 1.7 μm. This threshold is likely determined through absorption heating caused by impurities [40]. The pure fused silica core of the SCPBGF can be manufactured with fewer impurities compared to doped-core fibers which have been shown to permit at least 13 W/μm<sup>2</sup> (2 kW CW in a 14 μm mode field diameter beam) [1]; therefore it is reasonable to expect that higher CW intensities are possible in an un-doped core. Incorporation of this type of fiber into a Raman oscillator

may be complicated by the fact that the higher gain modes within the cladding inclusion structure may reach threshold before the core mode depending on how the cavity reflectors are configured.

At such high intensities the third order nonlinearity of the fused silica may cause spectral broadening through self phase modulation, cross phase modulation, and four wave mixing. If a single frequency seed source is considered, the anomalous dispersion of the guided core mode gives rise to modulation instability [39] however as previously mentioned the seed source must be broad enough to mitigate SBS. The calculated dispersion of this fiber is shown in Fig. 7. For wavelengths near the center of the band gap, the waveguide contribution to the dispersion is negligible as expected for a weakly guiding fiber. At the first Stokes wavelength the total dispersion is slightly higher than the material dispersion. Approaching the band gap, the total dispersion rises severely as the waveguide contribution begins to dominate.

Techniques developed to treat continuous wave fiber supercontinuum sources apply to the present situation. The main differences are that the spectrum of the first Stokes is too narrow to cause intra-pulse Raman amplification of spontaneously generated solitons and the ~50 nm width of the Raman gain spectrum limits the maximum amplified spectral width. CW supercontinuum generation is highly dependent on the characteristics of the pump, which in the present case corresponds to the first Stokes seed [41]. This suggests that the temporal and spectral characteristics of the seed source may be optimized to mitigate broadening of the signal. Optical power that is shifted outside of the Raman gain bandwidth may still be guided within the core as long as it remains within the band gap. Optical power that is shifted outside of the bandgap is lost into cladding modes thus reducing the power in the core. Ultimately such non-linear effects will lead to some additional efficiency loss. A computational analysis of non-linear spectral broadening in SCPBGF, though beyond the scope of this paper, may be required in the future.

## 5. Conclusion

Solid core photonic bandgap fibers incorporating graded index inclusions enable robust suppression of the second Stokes wavelength in the core of cladding-pumped Raman fiber amplifiers enabling efficient optical conversion of the pump to the first Stokes wavelength. Additional requirements for realizing such amplifiers include high power single mode pump sources, an efficient method of launching the pump and seed, careful attention to the packaging of the fiber, and very low optical loss in the fiber. An amplifier simulation incorporating this type of fiber exhibited an output power of 85 kW with 78% optical conversion efficiency under realistic assumptions.

## Acknowledgments

This work was supported in part by a grant of computer time from the DOD High Performance Computing Modernization Program at the Maui High Performance Computing Center. The author gratefully acknowledges Dr. Iyad Dajani for helpful discussions, Dr. Kyle Gresham for incorporating this work into the research electives portion of the Air Command and Staff College curriculum and the High Energy Laser Joint Technology Office, the Air Force Research Laboratory Directed Energy Directorate, and the Laser and Optics Research Center at the United States Air Force Academy for support.